

Uncertainty analysis for rolling contact fatigue failure probability of silicon nitride ball bearings

Sriram Pattabhiraman, George Levesque, Nam H. Kim, Nagaraj K. Arakere *

Department of Mechanical and Aerospace Engineering, University of Florida, Gainesville, FL 32611, USA

ARTICLE INFO

Article history:

Received 17 January 2010

Received in revised form 3 May 2010

Available online 25 May 2010

Keywords:

Ball bearings

Ceramics

Contact

Finite element modeling

Friction

Hybrid bearings

Partial cone crack

Rolling contact fatigue

Stochastic

Stress intensity factor

Silicon nitride

Surface crack

Uncertainty

ABSTRACT

Uncertainty analysis and parametric studies are presented for estimating the fatigue failure probability of surface cracks in silicon nitride ball bearings subjected to rolling contact fatigue. Uncertainty quantification of input parameters are presented first based on experimental data, inspection capability, and geometric reasoning. Surrogate models for equivalent stress intensity factors are then used for uncertainty propagation, which are built upon high fidelity finite element modeling with half-penny-shaped surface cracks. Instead of black-box type surrogate modeling, physical observations are employed to decompose the high dimensional surrogate model into multiple one-dimensional models. The cross-validation technique is used to find the best surrogate that has the smallest prediction variance. The probability of failure is estimated using Monte Carlo simulation and surrogate models. The parametric studies show that reducing the maximum crack size (by limiting inspection threshold) and increasing the fatigue threshold (by improving fracture toughness of a material) are the most effective ways of reducing the probability of failure. For example, decreasing the maximum crack size by 4.4% and increasing the lowest fracture threshold by 2.8% results in the reduction of probability of failure by 40%. Ball survivability increases with decreasing ball diameter, for a given peak Hertzian stress. In order to apply the current study to hybrid ball bearing design, the survivability results are generalized through non-dimensionalization.

© 2010 Elsevier Ltd. All rights reserved.

1. Introduction

Ball and roller bearings are widely used in a variety of industrial machinery to allow relative motion and support load in rotating shafts. In conventional ball bearings, with metal raceways and balls, subsurface-originated spalling and surface-originated pitting have been recognized as the dominant modes of failure due to rolling contact fatigue (RCF) (Sadeghi et al., 2009). Bearing subsurface material is subjected to RCF cycles that induces a complex triaxial stress state, non-proportional loading, high hydrostatic stress component, and changing planes of maximum shear stress during a loading cycle, and eventually leads to a subsurface crack. The spalling failure occurs when subsurface cracks propagate towards the surface to form a surface spall (Sadeghi et al., 2009). This mechanism is the dominant mode of failure in rolling element bearings that have smooth surfaces and operate under elastohydrodynamic lubrication (EHL) conditions. Surface originated pitting occurs in cases where surface irregularities in the form of dents or scratches are present. Here, cracks initiate at the surface stress concentrators and thereafter propagate at a shallow angle to the surface (Bower, 1988). This

mechanism of failure is more common in gears where substantial sliding occurs between the contact surfaces.

Aircraft engine manufacturers have been aggressively pursuing advanced materials to meet main-shaft bearing requirements of advanced engines for military, commercial and space propulsion. These requirements include bearings with extended life, superior corrosion resistance, surface durability and tribological performance. Hybrid bearings, which utilize silicon nitride balls and steel raceways, have been tested to have considerably longer fatigue lives, to have superior thermal behavior, to last up to five times longer in oil starvation conditions (Miner et al., 1996; Tanimoto et al., 2000) and to perform well under corrosive conditions (Klemm, 2002). Silicon nitride balls have many desirable physical properties that allows for advancing bearing technology including low density and high compressive strength but also have low fracture toughness of 4–6 MPa $\sqrt{\text{m}}$ (Piotrowski and O'Brien, 2006). This low fracture toughness, in combination with unavoidable ball-to-ball collisions in the manufacturing (lapping) process often results in ring or c-cracks (partial cone cracks) (Cundill, 1997). These flaws can grow under RCF when placed in service and result in a spall on the ball surface, as shown in Fig. 1 (Levesque and Arakere, 2008).

The failures caused by surface cracks of silicon nitride ball bearings under rolling contact have been addressed by 'ring or c-cracks'

* Corresponding author. Tel.: +1 352 392 0856; fax: +1 352 392 1071.

E-mail address: nagaraj@ufl.edu (N.K. Arakere).

Nomenclature

a	crack semi-width	N_C	number of simulation samples that lie in the contact patch
a_{mean}	mean crack semi-width	p_o	max elliptical contact pressure
a'	semi-major axis of elliptical contact patch	P_F	probability of failure
b	crack length	R	radius of ball
b'	semi-minor axis of elliptical contact patch	r_d	radial position of crack face nodes
d	diameter of ball	u_i, v_i, w_i	displacements of crack face nodes
E	Young's modulus	ν	Poisson's ratio
g	limit state function	x_d	elliptical contact patch x-coordinate
I_j	index function	x_D	lateral position of crack to contact patch center
K_{eq}	equivalent stress intensity factor from CSERR	y_d	elliptical contact patch y-coordinate
K_I	opening crack tip stress intensity factor	μ	friction coefficient
K_{II}	sliding crack tip stress intensity factor	ϕ	crack orientation,
K_{III}	tearing crack tip stress intensity factor	σ_{PF}	standard deviation of the probability of failure
K_{th}	fatigue threshold	z, θ	spherical coordinates at the center of ball bearing
N	number of Monte Carlo simulation samples		
N_f	number of simulation samples that fail		

(Hadfield, 1998; Hadfield and Stolarski, 1995; Hadfield et al., 1993; Kida et al., 2004; Wang and Hadfield, 2000a,b, 2001; Wang et al., 2000) and 'wedge effect' models (Chen et al., 1996). In the *c*-crack model, the Hertzian contact stresses occurring around the perimeter of the bearing contact area are thought to dominate the crack growth. The lubricant is assumed to have no effect on the crack growth. In the wedge effect model, the fluid pressure is thought to penetrate into the crack by contact pressure. When the fluid is pressurized by the maximum contact pressure at the contact center it is thought to cause crack growth. The mechanisms of these two models have been investigated separately. A surface crack is likely to be affected by the stresses used in both models as a ball passes over the crack (Oguma et al., 1997; Wang and Hadfield, 1999). The stress intensity factor (SIF) at the crack tip is also adversely affected by the presence of friction-induced traction forces at the contact. However, effects of the fluid pressure are not well understood or characterized yet and the dominant mode of failure is thought to be crack growth driven by SIFs arising from the contact patch passing over the *c*-crack (Hadfield, 1998; Hadfield and Stolarski, 1995; Hadfield et al., 1993; Oguma et al., 1997; Wang and Hadfield, 1999, 2000a,b, 2001; Wang et al., 2000). Partial cone or *c*-cracks are considered the most damaging surface defect that limits ball life in hybrid bearings under service conditions (Evans, 1983; Hadfield et al., 1993).

The fatigue damage process in ceramic rolling elements is very different from metal balls. RCF in metal bearings is manifested as a

flaking off of metallic particles from the surface of raceways and/or rolling elements. As described earlier, this process commences as a crack *below* the surface and is propagated to the surface, eventually forming a pit or *spall* in the load-carrying surface (Harris, 1991). Bearing fatigue life estimation is still largely based on the seminal probabilistic life model by Lundberg and Palmgren (LP) (1947), first proposed in 1945. Despite many improvements to the LP model current probabilistic bearing life prediction methods are based on the ISO standard set up in 1989 (ISO, 1989) and continue to rely on extensions to the LP model, are empirical in nature, and include variables that are obtained from extensive experimental testing. The LP theory states that for bearing rings subjected to N cycles of repeated loading the probability of survival S is given by,

$$\ln \frac{1}{S} = A \frac{N^e \tau_0^c V}{z_0^h} \quad (1)$$

where τ_0 is the maximum orthogonal shear stress in the contact region, z_0 is the corresponding depth at which this stress occurs, and V is the stressed volume of material. The parameters A , c and h are material characteristics that are determined experimentally. The parameter e is the Weibull slope for the experimental life data plotted on a Weibull probability paper.

Metals are weaker in shear than tension. In contrast to metallic materials, Si_3N_4 material is weaker in tension than compression or shear. The LP model cannot account for this difference in material

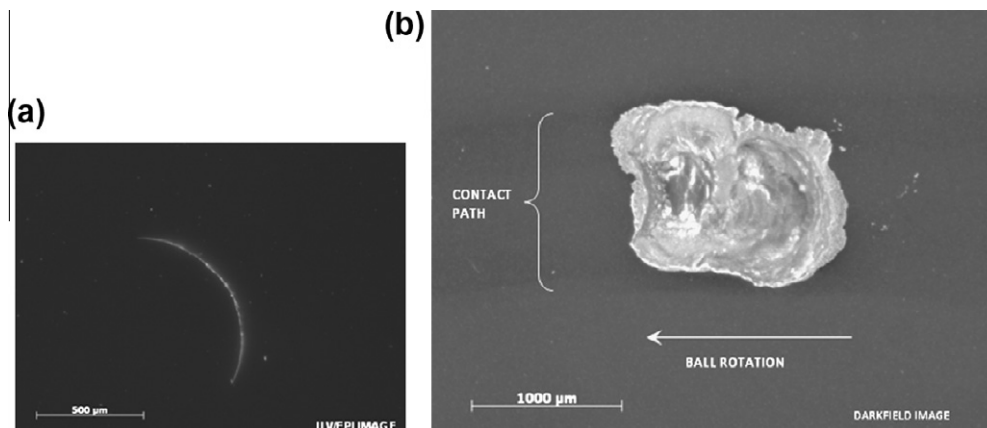


Fig. 1. (a) A partial cone or *c*-crack on a silicon nitride ball surface. (b) The *c*-crack subjected to rolling contact fatigue in a ball bearing, resulting in crack growth and spalling. The contact path (ball track) whose width is $2a'$ is faintly visible. [Image courtesy of The Timken Company.]

behavior. Furthermore, *c*-cracks already exist on the ball surface and hence subsurface crack initiation and subsequent growth to a spall is not pertinent to ball failure. Instead, a fracture mechanics methodology that evaluates the *critical flaw* size in balls is required, since failure typically occurs, for hybrid bearings rolling elements, when the equivalent SIF at the crack tip equals the mixed-mode fracture toughness of the silicon nitride ball material.

The largest allowable surface flaw that does not propagate under RCF loading is of design significance, and is termed the *critical flaw size* (CFS). A systematic procedure to compute the CFS based on fracture mechanics principles, RCF loading, and ball material properties has been recently presented by Levesque and Arakere (accepted for publication). Non-destructive evaluation (NDE) techniques are being developed and used on each ball in order to determine if it is acceptable to enter service (Wang, 2000). The resolution to which each ball is inspected, as determined by the CFS, has a strong effect on the cost of each ball and has been analyzed deterministically in prior work (Levesque and Arakere, accepted for publication). The cost of NDE method for silicon nitride balls scales up very steeply with decreasing CFS and increasing ball diameter. Thus the cost associated with NDE can become a significant fraction of the overall manufacturing cost of the silicon nitride ball.

Brittle materials inherently exhibit considerable variation in material mechanical and fracture properties. For example, there is a significant variation in the depth of a surface crack from a controlled impact (Lawn, 1994). Also there is a noted variation in the specimen to specimen fracture toughness (for example 4.85 ± 0.36 MPa $\sqrt{\text{m}}$, Piotrowski and O'Brien, 2006). Hence, there can be considerable variation in the surface dimension, depth, shape and distribution of surface cracks produced by unavoidable collisions during the manufacture of silicon nitride balls (Wang, 2000).

In general, predicting fatigue failure of a ball bearing requires probabilistic approaches due to various uncertainties in system parameters, including uncertain size, location, and direction of cracks; variability in material properties; and uncertainty in applied loads. Uncertainty in the system parameters makes it computationally expensive to evaluate the safety (or reliability) of the system due to the significant number of analyses required in the traditional Monte Carlo simulation (MCS). Critical issues for overcoming these difficulties are those related to uncertainty quantification and uncertainty propagation. Traditional approaches for these tasks often fail to meet constraints (computational resources, cost, time, etc.) typically present in industrial environments. In order to overcome this limitation, several alternatives are presented, such as the first- and second-order reliability method (FORM/SORM) (Melchers, 1999), the inverse reliability method (Tu, 1999), the importance sampling method, MCS using response surface (Qu and Haftka, 2004), stochastic response surface method (Kim et al., 2006a), etc. Although every method has its own strengths and limitations, MCS using response surface is utilized in this paper because it provides a convenient way of evaluating reliability with reasonable accuracy. Especially when the bounds of input random variables are relatively small, the accuracy of response surface approximation is good and thus the estimation of reliability. The weakness of response surface is the so-called curse of dimensionality; the number of required simulations increases rapidly and in proportion to the number of input variables (Kim et al., 2006b). However, when the input variables are not correlated or the correlation is not strong, this difficulty can often be reduced by decoupling these variables.

This paper presents a comprehensive procedure for uncertainty analysis and parametric studies for estimating the fatigue failure probability of surface cracks in silicon nitride ball bearings subjected to RCF. The paper is organized as follows. In Section 2, the finite element modeling technique for computing mixed-mode

stress intensity factors at surface crack tips subject to RCF is presented. In Section 3, uncertainty analysis using the RCF results is presented in separate subsections. In Section 3.1, the uncertainty quantification in hybrid bearings is outlined. Section 3.2 explains how to choose the best surrogate model using cross-validation. Uncertainty propagation is performed using Monte Carlo simulation and surrogate models in Section 3.3. In Section 3.4, the effect of crack size and fatigue threshold improvement on ball survivability is presented. In Section 3.5, the ball survivability results are presented in terms of non-dimensional variables so that they can be applicable for design. Conclusions are presented in Section 4. The results are of immediate interest and relevance to hybrid ball bearing and turbine engine manufacturers.

2. Modeling RCF orientation effects on surface crack SIFs

The radius of *c*-cracks produced during ceramic ball-to-ball interactions is proportional to the ball radius, *R*. Also, the velocity needed to induce *c*-cracks has been shown to be proportional to R^3 (Levesque and Arakere, accepted for publication). The range of possible crack shapes and sizes has been established by Levesque and Arakere (2008). The angular extent of the *c*-cracks on the surface of the ball is roughly 90–120° (Wang, 2000). The resultant nonplanar crack shape from ball-to-ball interactions is complex and leads to a difficulty in generalizing results and in finding which geometry of crack will be the most severely affected by RCF (Levesque and Arakere, 2008). The complex nonplanar 3D geometry of the *c*-crack requires parameters such as crack depth and angle to surface, which are difficult to measure. Furthermore, the NDE inspection procedures can reliably only detect the chord length of the crack on the ball surface. With these issues in mind, the worst-case SIFs produced by an elliptical contact with peak Hertz stress, p_o , rolling over a nonplanar *c*-crack and a semi-elliptical flaw has been compared by Levesque and Arakere (accepted for publication). The semi-elliptical flaw is fully classified by three parameters (depth, width, and angle of inclination). The semi-elliptical crack with a width ($2a'$) equal to the chord length of the *c*-crack, and same depth and inclination angle was found to generate higher peak SIFs, for the same peak Hertz stress, P_o , leading to a conservative analysis. Having established that semi-elliptical surface cracks subjected to rolling contact loading results in higher crack tip loading and SIFs, we present the numerical procedure for computing SIFs via FEA.

Finite element analysis techniques have been developed to analyze 3D surface flaws subject to rolling contact loads typically seen in ball bearing raceway elliptical contacts, for mixed-mode stress intensity factor (SIF) calculation (Levesque and Arakere, 2008, accepted for publication). SIF calculation is done by the crack tip opening displacement correlation method.

SIF calculation is conducted on RCF models for a crack whose width is 250 and 75 μm depth angled 30° to the surface. These specific dimensions were chosen since they have been experienced to be a set of dimensions that have been observed in experiment (Wang, 2000) and have exhibited high SIFs when compared to other geometries (Levesque and Arakere, accepted for publication). Loading is done via FORTRAN user subroutines DLOAD and UTRACLOAD for ABAQUS (Dassault Systèmes, 2007) for normal and traction loads. The equations to describe the Hertzian pressure distributions in the contact patch can be written as:

$$p(x,y) = p_o \sqrt{1 - \left[\frac{(x - x_d)^2}{a^2} + \frac{(y - y_d)^2}{b^2} \right]} \quad (2)$$

and

$$f(x,y) = \mu p(x,y) \quad (3)$$

where p_o is the peak Hertzian pressure, x_d and y_d are the distances from the global coordinate system to the load center, a' and b' are the semi-major and semi-minor axes of the contact patch, respectively, and μ is the friction coefficient for the moving load in a full-slip interaction (see Fig. 2). For the specific cases that were run we used an elliptical load aspect ratio of 1/8 and a $\mu = 0.07$ which is representative of elasto-hydrodynamically lubricated ball bearing contacts in aerospace applications.

The SIFs are calculated in all three modes, at every point along the semi-elliptical crack front. For implementation in determining what combination of these three modes of crack displacement has met a fatigue threshold, or K_{th} , we utilize (Levesque and Arakere, accepted for publication) the critical strain energy release rate (CSERR) as adapted from Anderson (2005) and can be written as

$$K_{eq} = \sqrt{K_I^2 + K_{II}^2 + (1 + \nu)K_{III}^2} \quad (4)$$

For initiating brittle fracture along the crack front, the maximum value of K_{eq} is considered important. Consequently we have taken the SIFs, calculated as a function of crack tip position, and combined them into a single parameter (using Eq. (4)) and have then chosen the highest value along the crack front as the representative value to determine if crack growth can occur for each orientation.

For the uncertainty analysis, we must be able to calculate the highest K_{eq} for a randomly oriented crack relative to the moving contact patch. For a given combination of radial load, thrust load and speed, the ball bearing typically has a fixed contact angle and hence the ball track, whose width is determined by the length of the contact ellipse major axis, traverses the ball, as shown schematically in Fig. 3. The contact patch therefore passes on the ball surface in a band and does not change direction for the entire sequence. The load magnitude and the traction magnitude and direction do not change relative to the elliptical contact. As the load passes around the ball, there exists only one position where the max SIF is reached and this orientation is nearest to the contact patch and on the opposite side of the traction direction. This maximum position can be classified with two variables: the lateral position of the crack relative to the center of the contact patch, x_D , and the angle that the crack makes on the surface relative to the contact patch tangent, ϕ . We treat the distance of the crack to the center of the contact load in the y_D direction as always 0 for maximum SIFs (see Fig. 2). We have run parametric studies for these two parameters and separated their effect as independent

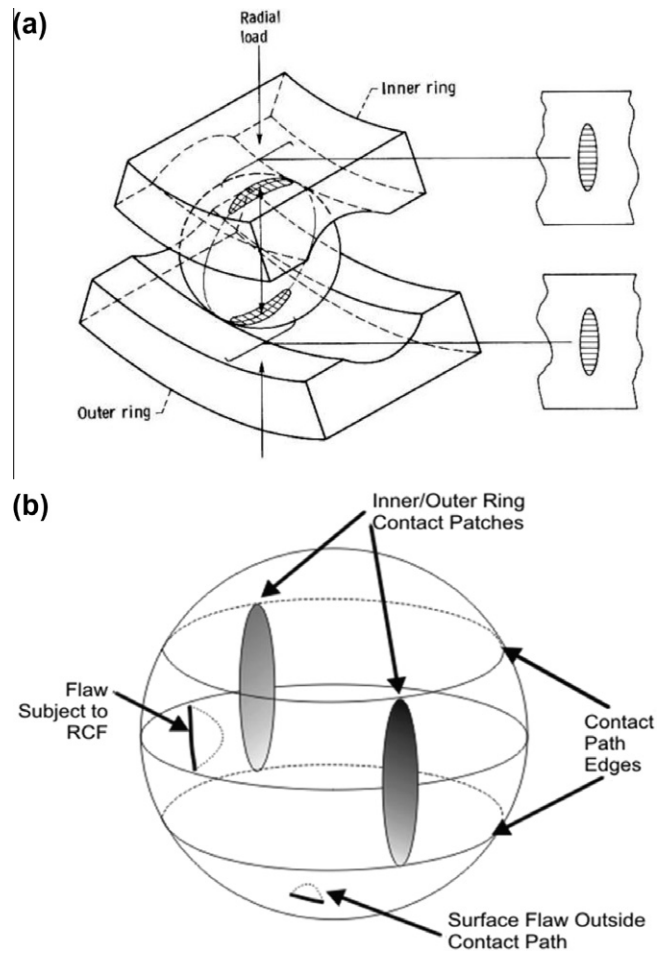


Fig. 3. (a) Elliptical Hertzian contact patches between the ball and bearing raceway surfaces in a radially loaded bearing (Hamrock and Dowson, 1981). (b) Schematic of the ball surface subjected to RCF within the ball track as the ball rolls at a fixed contact angle. Cracks inside and close to this region will experience RCF from the Hertzian stress/displacement field.

parameters in Figs. 4 and 5. When contact angle changes due to load and speed changes, a new equilibrium position is reached,

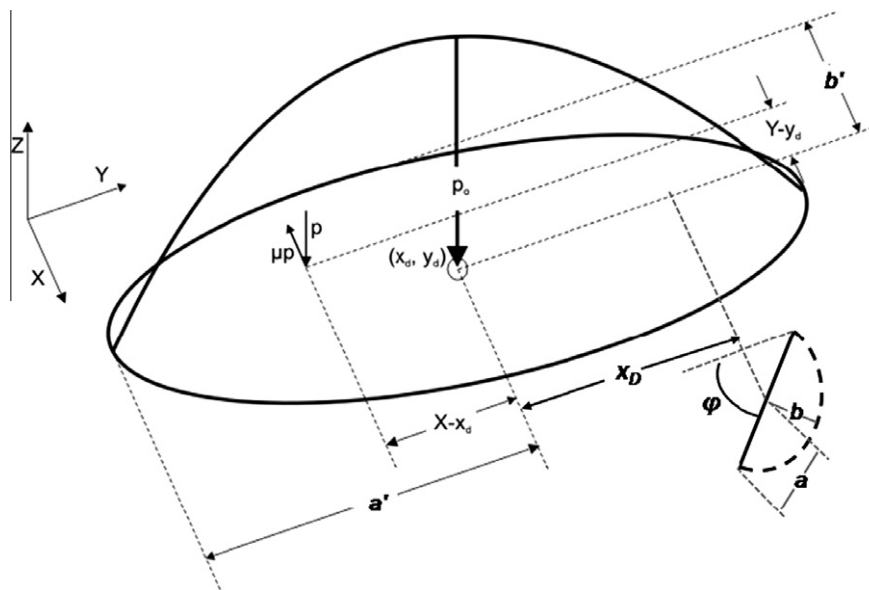


Fig. 2. Semi-elliptical surface crack (dimensions a , b and orientation ϕ) in relation to the elliptical Hertzian rolling contact (dimensions a' and b') load.

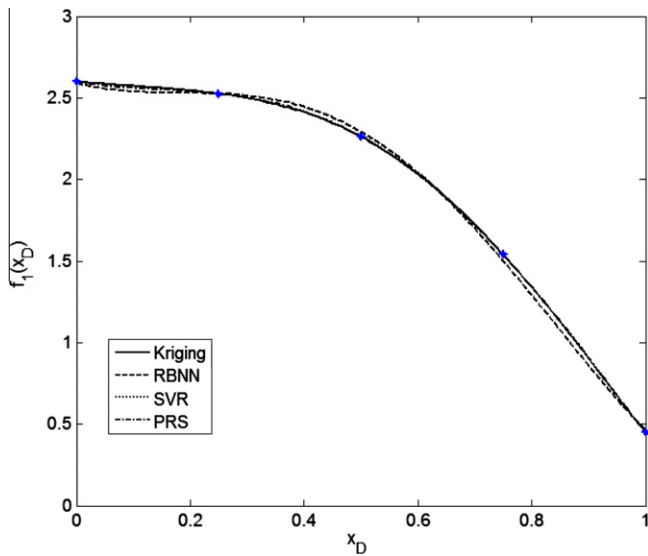


Fig. 4. Surrogate models for the contribution of lateral position to the stress intensity factor.

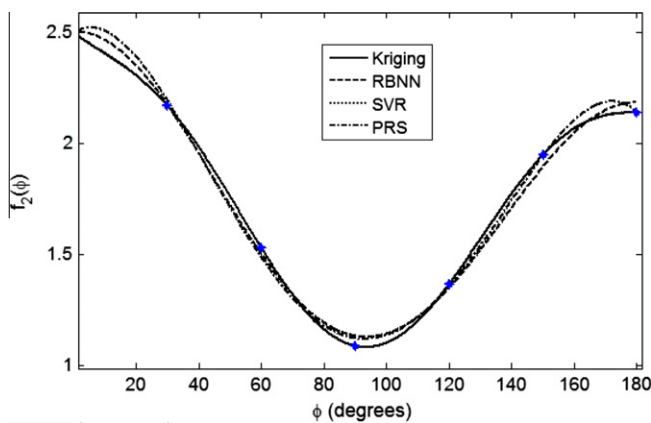


Fig. 5. Surrogate models for the contribution of crack orientation to the stress intensity factor.

with different ball track width that traverses a different region of the ball and Hertzian stress p_o . Over the life of the ball the entire region of the ball is likely traversed by the ball track and thereby potentially subjecting the surface cracks distributed over the ball surface to RCF. The probability of failure will depend on p_o , the relative orientation and size of cracks, and their statistical distribution with respect to the ball track.

3. Uncertainty analysis

In this section, uncertainty analysis for estimating the failure of silicon nitride ball bearings is presented using surrogate modeling and Monte Carlo simulation. The fatigue failure model in the previous section is based on the equivalent SIF, which depends on the size, direction and location of a crack; fracture toughness of the material; and applied loads. However, it is difficult to determine if a bearing may fail or not because there are many uncertainties in the practical operating environment. For example, an existing crack may not fail if its location is out of the contact patch or its size is too small to fail. Thus, the failure of a bearing can only be evaluated in terms of probability. The goal of this section is to evaluate the probability of fatigue failure of silicon nitride ball bearings under representative operating conditions.

3.1. Uncertainty quantification

The first step in uncertainty analysis is to quantify uncertainty in input parameters. Table 1 summarizes input parameters that are used in uncertainty analysis. Some parameters are considered to be deterministic, while the others are random. Even if all bearings do not have the same diameter due to manufacturing tolerances, it is considered a deterministic value because its contribution to the uncertainty in fatigue failure is also small. In general, the uncertainty in the applied load is large and difficult to characterize. In fact, it is known that the applied load is the largest source of uncertainty. However, a deterministic value of the maximum applied pressure of $p_o = 2.7$ GPa (392 ksi) is used in uncertainty analysis due to the following two reasons: first, it is difficult to characterize probabilistic distribution of the applied load, and second, it will provide conservative estimate of the probability of failure due to the relatively high peak Hertzian pressure used.

Major uncertainties are related to the crack configuration. Based on inspection data (Cundill, 1997), a new silicon nitride ball bearing can have many micro-cracks on the surface. Levesque and Arakere (2008, accepted for publication) showed that these cracks can be modeled using half-penny-shaped cracks with a specific size, aspect ratio and orientation. Since the manufacturing process does not have any preference in the orientation of nucleated cracks and ball orientation in the assembly can vary often, it is assumed that they are uniformly distributed between 0° and 180° . For the same reason, the location of crack is also uniformly distributed on the ball surface. Based on sample measurements by Wang (2000), it is reported that the initial crack size can be between 200 and 350 μm . Since no probabilistic distribution information is available, it is assumed that the initial crack size is uniformly distributed between the minimum and maximum sizes. In the perspective of fatigue failure, the lower bound is not significant. On the other hand, the upper bound depends on manufacturing and inspection methods, which is also related to the cost.

Piotrowski and O'Brien (2006) have evaluated the fracture toughness value for silicon nitride ball material when an applied force generates a tensile hoop stress on a pre-cracked ball. The fracture toughness value, computed from 16 experiments shows a uniform variation within 12% of the nominal value. Thus, the uncertainty of the fatigue threshold is modeled using a uniform distribution with the nominal value of $2.8 \text{ MPa}\sqrt{\text{m}}$ and is in the suggested range of 2–4 $\text{MPa}\sqrt{\text{m}}$ (Wang, 2000). In the sensitivity study, the effect of these parameters will be discussed.

3.2. Surrogate modeling – cross-validation

In the uncertainty propagation stage, the input uncertainties are propagated through the governing physics of the system to yield uncertainty in output, which is the equivalent SIF. Traditionally, Monte Carlo simulation (MCS) is often employed for this purpose, in which many samples of input random variables are generated according to their distribution types, and samples of output variable are produced by solving the governing equation with each set of input variables. This stage is computationally intensive because it involves 3D finite element modeling and volume integrals. For example, for given values of input parameters, the computation of equivalent SIF takes about 1300 s in desktop computer with two processors. In order to identify the effect of input uncertainty on the output uncertainty, numerous repetitions of this calculation are required, which becomes impractical easily. Thus, the key issue in uncertainty analysis is how to effectively propagate the input uncertainty to the output uncertainty.

There are many methods available in uncertainty propagation using approximation. First-order reliability method (FORM) (Allen

Table 1
Input parameters and their distributions for uncertainty analysis.

Parameter	Type	Value (or distribution)
Diameter of ball, d	Deterministic	25 mm
Width of contact patch, b'	Deterministic	8 mm
Pressure, p_0	Deterministic	2.7 GPa (392 ksi)
Friction coefficient, μ	Deterministic	0.07
Fatigue threshold, K_{th}	Random	$U[2.46, 3.14]$ MPa \sqrt{m}
Crack semi-width, a	Random	$U[200, 350]$ μm
Crack orientation, ϕ	Random	$U[0^\circ, 180^\circ]$
Crack position, x_D	Random	Uniformly distributed on the sphere

and Camberos, 2009), second-order reliability method (SORM) (Allen and Camberos, 2009), importance sampling method (Cano et al., 1996), and MCS are a short list of available methods. Except for MCS, all other methods use approximation in either output variable or its distribution, which inevitably involves error especially when the governing system equation is complex. In this paper, surrogate modeling techniques (Viana, 2009) are utilized to approximate the relation between input parameters and output. Instead of black-box type surrogate model, physics-based surrogate modeling is employed to represent the relationship more effectively. Once the surrogate model is obtained, uncertainty in output variable can easily be calculated using MCS because the computational cost of function evaluation using the surrogate model is negligible.

The equivalent SIF for cracks on ball bearings is characterized with four parameters: applied contact pressure, lateral position of crack with respect to center of contact patch, orientation of crack, and initial crack size. Thus, the functional relationship can be written in a general form of

$$K_{eq} = f(p_0, x_D, \phi, a) \quad (5)$$

where p_0 is the applied pressure at the center of contact patch, x_D is the normalized lateral position between the center of contact patch and the center of crack, ϕ is the angle between a line perpendicular to the contact path and the orientation of crack, and a is the semi-width of surface crack. Although the explicit expression of function f is unknown (or, sometimes it is an implicit function), it can be evaluated for given input parameters using finite element analysis and volume integrals.

The idea of surrogate modeling is to approximate the function f using a simple analytical function (Queipo et al., 2005). The general procedure of surrogate modeling is to generate several samples, called design of experiment, and to fit a function using these samples. First, a number of samples are chosen based on different criteria, such as full factorial design or Latin hypercube sampling. The larger the sample size, the better the quality of approximation. However, each sample requires expensive finite element analysis. In order to have a reasonable accuracy, the number of samples for the case of four variables will be around 100. The number of required samples exponentially increases as the number of input variables increases. Once all samples are available, they are used to fit a function. In general, the functional form is fixed with unknown coefficients, which are to be found by minimizing the error between the function and samples.

In general, surrogate modeling does not require detailed knowledge on the physical problem; it can be considered as a black-box. In this paper, however, the surrogate model is simplified by observing the physical behavior of the system, in which the equivalent SIF can be expressed as a function of the four parameters in the following form:

$$K_{eq} = \frac{p_0}{2700 \text{ MPa}} \times f_1(x_D) \times \frac{f_2(\phi)}{2.5} \times \sqrt{\frac{a}{250 \mu m}} \quad (6)$$

First, the SIF, K_{eq} , is proportional to the contact pressure because the material response is linear elastic and stress increases linearly with the applied load. In addition, K_{eq} is proportional to the square root

of crack length which is basically identical to the traditional definition of SIF. Since these two relations are simple and explicit, there is no need to introduce approximation using surrogate modeling. On the other hand, the effects of lateral position and orientation are not straightforward, and thus, require approximation. An important point in the above equation is that the effects of these two parameters are decoupled. This can be explained by considering two cracks located in different lateral positions for which the failure mechanism will still be the same except that the magnitude of contact periphery stress will be different. In the above equation, it is assumed that the aspect ratio of the semi-elliptical crack, the cracks angle to the surface and the elliptical contact patch aspect ratio remain constant.

After simplifying the relationship between input variables and output, the initial surrogate model with four variables can now be simplified to two surrogate models with a single variable, which is much more computationally efficient to build and more accurate. To simulate the variation in SIFs due to orientation, seven equally-spaced simulations are generated for the orientation angle and five for the lateral position within their ranges and are interpolated between for computational accuracy.

The next step is to choose a surrogate model. The difficulty is that there is no single surrogate that outperforms all others. Depending on functional behavior, one surrogate performs better than the others. In general, however, the functional behavior is unknown a priori. One of the best practices is to build multiple surrogates using the sampled data and choose the best one. It is generally accepted that cross-validation (Myers and Montgomery, 2002) is a good tool to choose the best surrogate. This procedure is relatively inexpensive under the assumption that obtaining a sample requires expensive finite element analysis, but surrogate modeling can be finished without requiring intensive computation. In this paper, four surrogates are considered: Kriging, Radial Based Neural Network (RBNN), Support Vector Regression (SVR), and fourth-order polynomial response surface (PRS). Different surrogates have different characteristics. For example, the Kriging always pass the sampled data points, while PRS does not pass the data point exactly. However, that does not mean that the former is more accurate than the latter. The accuracy of a surrogate should be measured at data points that are not used in fitting the surrogate.

Figs. 4 and 5 show the approximation of $f_1(x_D)$ and $f_2(\phi)$, respectively, using four different surrogate models. Since all four surrogates are close to each other, it is difficult to tell which surrogate is the best. Without having additional test points, cross-validation can be used to find the best surrogate. In cross-validation, one data point is dropped in fitting the surrogate and the error is measured at the dropped data point, which is called a prediction error. If this procedure is repeated for all data points, the root mean square of prediction errors (PRESSRMS) can be used as an indicator of accuracy. PRESSRMS is a well established parameter to compare the effectiveness of surrogates. The smaller the PRESSRMS value is, the more effective the surrogate is.

Table 2 compares the PRESSRMS values for all four surrogate models. It shows that Kriging is a good model to fit the lateral position, while PRS is good for the orientation.

3.3. Uncertainty analysis – Monte Carlo simulation using surrogate

Once surrogate models are selected, they can be used to evaluate the uncertainty of SIF according to the uncertainty in input parameters. Since function evaluation in the surrogate model is very fast, MCS can be used for that purpose. The procedure is to generate many samples of input parameters according to their distribution types and to apply them to the surrogate model to generate samples of SIFs. From the data in Table 1, it is relatively straightforward to generate samples of uniformly distributed crack sizes and orientations using a random number generator. However, generating samples of lateral positions is not straightforward because they are uniformly distributed on a sphere.

The method to uniformly distribute points on a sphere is based on Archimedes theorem, which is stated as “the axial projection of any measurable region on a sphere on the right circular cylinder circumscribed about the sphere preserves area.” The physics behind this theorem is explained in the Shao and Badler (1996). According to the theorem, two independent uniformly distributed random variables, $z \sim U[-1, 1]$ and $\theta \sim U[0, 2\pi]$ are sampled based on their distribution types. Each combination of (z, θ) corresponds to a sample of a point on the surface of the sphere, whose coordinates are given by

$$(x, y, z) = (\sqrt{1-z^2} \cos \theta, \sqrt{1-z^2} \sin \theta, z) \quad (7)$$

This method uniformly distributes points on the surface of a unit radius sphere. The normalized lateral position x_D in Eq. (6) is equivalent to x in Eq. (7) if the coordinate system is set such that the center line of contact patch is on the yz -plane. For dimensions in Table 1, the crack will be located within the contact patch if

$$|x_D| \leq \frac{b'}{d} \quad (8)$$

During MCS, a crack is located randomly on the surface of the ball bearing, whose lateral position is calculated from Eq. (7). If the crack lies within the contact patch according to Eq. (8), the equivalent SIF is calculated using Eq. (6).

The objective is to calculate the probability of fatigue failure of the silicon nitride ball bearing under input uncertainties described in Table 1. In this paper, the failure mode is defined when the equivalent SIF is larger than the fatigue threshold. For that purpose, a limit state function is first defined as

$$g = K_{eq} - K_{th} \quad (9)$$

and the probability of failure is defined by

$$P_F = \text{Prob}(g > 0) \quad (10)$$

In MCS, the probability of failure is calculated by counting the number of samples that are failed. When the total number of random samples is N , the probability of failure can be calculated by

$$P_F = \frac{1}{N} \sum_{j=1}^N I(g_j) = \frac{N_F}{N} \quad (11)$$

where I is an index function whose value is one when the argument is positive and zero otherwise, and N_F is the number of failed sam-

ples. Due to the random nature of MCS, different sets of samples may yield different values of probability of failure; exact P_F can only be calculated when the number of samples approaches infinity. The standard deviation of the probability of failure can be estimated using

$$\sigma_{PF} = \sqrt{\frac{P_F(1-P_F)}{N}} \quad (12)$$

Note that the standard deviation is inversely proportional to the number of samples. In a similar way, the probability of survival can be calculated by

$$P_S = 1 - P_F = 1 - \frac{N_F}{N} \quad (13)$$

It is noted that the P_S has the same standard deviation with P_F .

Table 3 shows the results of uncertainty analysis using MCS and surrogate modeling. In order to see the effect of samples, two different sets of samples are used: one with 10^5 and the other with 10^6 samples. Samples of the uncertain input parameters are randomly generated according to their distributions, and output samples of equivalent SIFs are calculated using Eq. (6). Since the fatigue threshold is also a random variable, the samples of equivalent SIFs are compared with that of fatigue threshold to determine the number of failure cases. In the table, N_C is the number of samples in which cracks are located within the contact patch, and N_F is the number of samples that fail. It is clear that the uncertainty in the probability, σ_{PF} , decreases as the number of samples increases. It can be concluded that for given uncertainties in input parameters, the chance that a ball bearing may fail is about 0.6%. In practice, the failure probability will be lower because the maximum applied Hertzian stress is used for p_0 .

The plot of cumulative distribution function (CDF) of the limit state function $g = K_{eq} - K_{th}$ for the case of 100,000 samples is shown in Fig. 6. In order to emphasize the failure probability, $1 - \text{CDF}$ is plotted in log-scale. The ordinate value at $g = 0$ is the value of failure probability. The discontinuity in the slope near $g = -2.5$ is due to the fact that those cracks lying outside the contact patch do not fail, and hence, do not contribute to the SIF calculation. As can be observed in the plot, the slope of the CDF curve near $g = 0$ is relatively high, which means that the failure probability can change significantly according to a small variation of the limit state function g . This can be achieved in various ways, such as using a material with higher K_{th} or reducing initial crack size that can reduce K_{eq} .

3.4. Parametric study

Even if the accuracy of the failure probability depends on uncertainty quantification of input parameters, it can still provide the possibility of improving the failure probability. An important question is how much the failure probability can be improved by modifying the input uncertainty. For example, the initial distribution of crack size was uniform between 200 and 350 μm . If the manufacturing technology is improved such that the largest initial crack size is reduced by 10%, then it would be beneficial to estimate how much the probability of failure can be improved. It is also possible to apply more strict inspection threshold, such that the maximum crack size can be reduced. In practice, it is not feasible to

Table 2
Cross-validation errors (PRESSRMS) for different surrogate models.

Model	PRESSRMS	
	Lateral position	Angular position
Kriging	0.1187	0.3921
RBNN	0.2597	0.1895
SVR	0.6224	0.4388
PRS	0.2308	0.1658

Table 3
Probability of failure values for different sample sizes.

N	N_C	N_F	P_F	σ_{PF}
100,000	67,816	557	5.57E-03	2.35E-04
1,000,000	679,338	5990	6.00E-03	7.71E-05

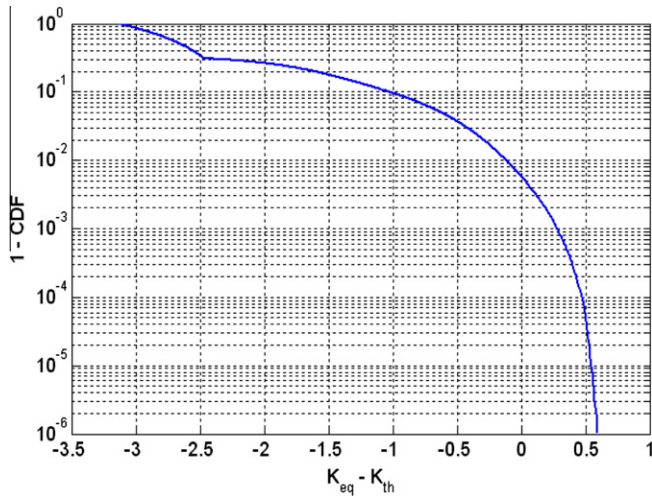


Fig. 6. Cumulative distribution function of the limit state function $g = K_{eq} - K_{th}$.

change the lateral position and the orientation of cracks as they are by nature random. However, the initial crack size and the fatigue threshold can be modified by using different manufacturing technology or different materials.

Table 4 compares the probability of failure when the initial distribution of crack size is reduced from $U[200, 350]$ μm (original) to $U[200, 335]$ μm (improved). Both cases use the same number of samples, 1,000,000. Note that reducing the largest initial crack size by only 15 μm (4.4%) improves the probability of failure disproportionately by 25%. A similar trend can be observed when the lowest fatigue threshold is increased by 0.07 $\text{MPa}\sqrt{\text{m}}$ (2.8%) such that the range is reduced from $U[2.46, 3.14]$ $\text{MPa}\sqrt{\text{m}}$ (original) to $U[2.53, 3.14]$ $\text{MPa}\sqrt{\text{m}}$ (improved). The effect of this improvement on the probability of failure is tabulated in Table 5, in which the probability of failure is improved by 24%. It is noted that improvement on fatigue threshold or crack size has a similar pronounced effect on the probability of failure. Table 6 shows the combined improvements when both the initial crack size and the fatigue threshold are improved. It turns out that the probability of failure can be improved by 40% due to these combined changes.

The variation of the probability of failure as a function of the largest initial crack size is shown in Fig. 7. It is noted that the probability of failure is very sensitive to the initial crack size. For example, when the largest initial crack size is reduced by 17% (from 350 to 290 μm) the probability of failure of the original material is decreased by 71% (from 0.006 to 0.0017). A similar improvement is observed for the material with higher fracture threshold. In order to isolate the effects of location and orientation of cracks, the probability of survival ($1 - P_F$) is computed for a deterministic crack size. The variation of the probability of survival as a function of crack size is shown in Fig. 8. Small crack sizes have a very high probability of survival. As the crack size increases, the probability of survival decreases and the decrease is less for a tougher material.

Piotrowski and O'Brien (2006) have measured the fracture toughness of aerospace quality silicon nitride ball bearings using radial compression of balls with a Vickers indented flaw and report

Table 4
Effects of improvements on probability of failure when the largest allowable initial crack size is reduced from 350 to 335 μm ($N = 1,000,000$).

Case	N_F	P_F	σ_{PF}
Original	5990	6.00E-03	7.71E-05
Improved	4548	4.50E-03	6.73E-05

Table 5
Effects of improvements on probability of failure when the lowest fatigue threshold is increased from 2.46 $\text{MPa}\sqrt{\text{m}}$ to 2.53 $\text{MPa}\sqrt{\text{m}}$ ($N = 1,000,000$).

Case	N_F	P_F	σ_{PF}
Original	5990	6.00E-03	7.71E-05
Improved	4563	4.60E-03	6.73E-05

Table 6
Effects of combined improvements on probability of failure when both crack size and fracture toughness are improved.

Case	N_F	P_F	σ_{PF}
Original	5990	6.00E-03	7.71E-05
Improved	3554	3.60E-03	5.95E-05

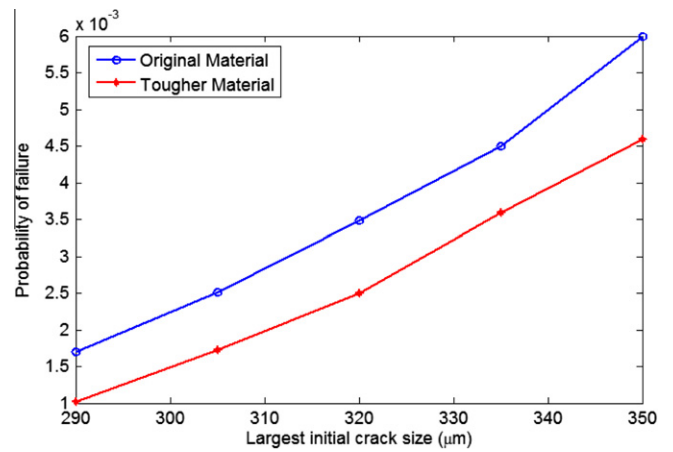


Fig. 7. Variation of probability of failure as a function of the largest initial crack size, for peak Hertz stress $p_o = 2.7$ GPa.

values at $\pm 12\%$ uniform variation about 4.5 $\text{MPa}\sqrt{\text{m}}$. We use this information to evaluate the variation of probability of survival as a function of crack size. The probability of survival as a function of crack size when the fracture toughness is 4.5 $\text{MPa}\sqrt{\text{m}}$ is shown in Fig. 9. Since the fracture toughness is much higher than that of Table 1, it allows the presence of much larger crack size with the same level of probability of survival. If an appropriate cost model is used for manufacturing and inspection methods, Figs. 7–9 can be used to select the optimum combination of material and NDE technique for the given level of safety of ball bearings.

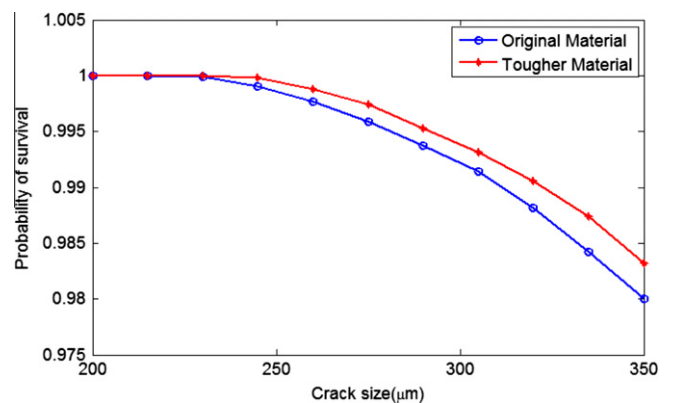


Fig. 8. Variation of probability of survival with crack size, for peak Hertz stress $p_o = 2.7$ GPa.

3.5. Generalization of survivability for different designs

Although the parameter studies in the previous section are performed only with a specific configuration, such as a single ball diameter and a single value of maximum pressure, they can be generalized to different configurations by non-dimensionalization so that the survivability results can be applicable to different designs of ball bearings. In particular, the following parameters are of interest in design: ball radius, R , crack semi-width, a , contact patch width, b' , and the maximum contact pressure, p_0 .

In the uncertainty analysis discussed in the previous section, the ball radius does not appear as a parameter, but it contributes indirectly to ball survivability via the maximum pressure, p_0 , the contact patch width, b' , and the crack semi-width, a . The contact patch dimensions, for a given Hertzian pressure p_0 , are a function of conformity between the ball and the inner and outer raceway radii of curvatures. For a given bearing support load a wide range of contact patch parameters can be selected based on bearing design preferences. In addition, the mean crack size is proportional to $R^{2/3}$. To generalize our results, we define and select a range of values for two non-dimensional parameters that are related to the contact patch area and K_{eq} .

The first non-dimensional parameter depends on the contact patch width (b') and circumference of the sphere. We note that the contact patch area is equal to $\pi a' b'$. Thus, a non-dimensional conformity parameter is defined as

$$c = \frac{2\pi R}{b'} \tag{14}$$

A lower value of c means greater conformity in the circumferential direction of the ball-raceway contact. In the numerical study below, we have selected a range of ball diameters varying from 4.763 mm (3/16") and 25.4 mm (1"), and the load ellipticity (b'/a') varies between 0.125 and 1.0, which can be converted into the conformity parameter between 9.82 and 78.54. We have included a wide range of ellipticities even though ratios close to 1.0 are not seen in ball bearings, but are encountered in ball-on-disc and other tribological tests.

Table 7 shows the values of parameters that are used in MCS in which four different bearing diameters and five different contact patch widths are considered. For any given ball size, there exists a range of possible contact patch ellipticities, for a given Hertzian stress p_0 . Since ellipticity of load directly influences the width of the contact patch band, it will affect ball survivability. To account for this effect, we normalize equation $f(x_D)$ for each contact patch width.

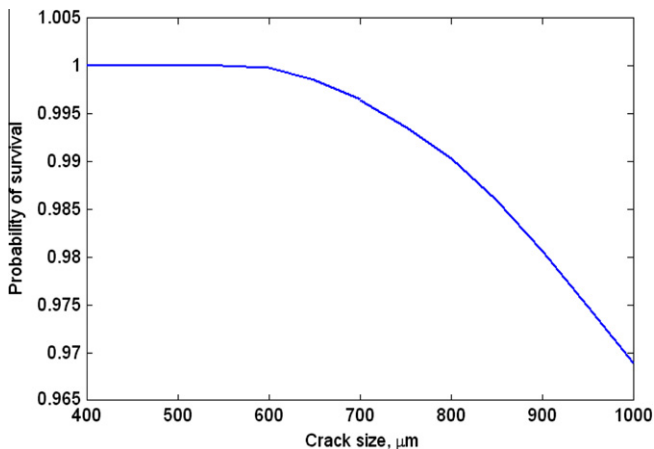


Fig. 9. Variation of probability of survival with crack size for a material with fatigue threshold 4.5 MPa \sqrt{m} , for peak Hertz stress $p_0 = 2.7$ GPa.

The second non-dimensional parameter is defined by normalizing the equivalent stress intensity factor with respect to bearing parameters of maximum contact pressure, p_0 , and mean crack size, a_{mean} , as

$$K_{eq}^* = \frac{K_{eq}}{p_0 \sqrt{a_{mean}}} \tag{15}$$

In the above definition, the fatigue threshold K_{th} is not included because often the same Si_3N_4 material with different grades may have different fatigue thresholds (Cundill, 1997). In addition, it is convenient to separate material parameters from geometric parameters for the purpose of uncertainty analysis. However, in order to evaluate the probability of failure or survival, the non-dimensional parameter K_{eq}^* has to be compared with the non-dimensional fatigue threshold, defined as

$$K_{th}^* = \frac{K_{th}}{p_0 \sqrt{a_{mean}}} \tag{16}$$

Fig. 10 plots the cumulative distribution of non-dimensional K_{eq}^* for five different values of conformity parameters. At each conformity parameter value, MCS with 1,000,000 samples is performed to calculate the distribution. Physical dimensions corresponding to each conformity value can be found in Table 7.

Reflecting on the plots in Fig. 10, a few general conclusions can be made. Firstly, as the ball diameter decreases survivability increases. This is due to the decreasing crack size since the mean crack size a_{mean} is proportional to $R^{2/3}$. In Levesque and Arakere (accepted for publication), the crack size was shown to scale with the bearing radius for normally colliding cone cracks. If 'partial cone' cracks are only portions of axi-symmetric cracks, the same proportionality may hold. As a result, bearing survivability can be independent of bearing size. However, if a_{mean} is proportional to R^x with $x > 1$, then larger balls are less likely to fail; whereas if $x < 1$, smaller balls are superior. The implications of this observation for bearing design are significant since for a given load the number of balls and ball diameter can be chosen to maximize ball life. Note that the assumed Weibull distribution of subsurface flaws, which is central to probabilistic bearing metal raceway life estimation techniques (Lundberg and Palmgren, 1947; ISO, 1989), does not hold here as it is not necessarily true that larger bearings will have more flaws as the random process that induces cracks could induce a similar number of flaws on any size bearings. In fact, one may argue that since the normal velocity to induce cracking of colliding spheres (which induces these flaws) is proportional to R^3 (Levesque and Arakere, accepted for publication), it is less likely for larger bearings to have the same number of flaws as their smaller counterparts.

In addition, as contact patch width, b' , increases ball survivability decreases because the contact band sweeps out more space on the ball and is thus more likely to have non-negligible crack tip displacement. For a 1" diameter Si_3N_4 ball, as $(2\pi R)/b'$ varies between 9.82 and 78.54, the survivability decreases only by 0.4%. Similarly, for a 5/8" diameter ball, a similar change in $(2\pi R)/b'$ leads to decrease in survivability by 0.01%. This conclusion is only true when the maximum contact pressure p_0 remains constant.

Table 7

The dimensionalized range of contact patch widths examined for the analyzed range of ball sizes. The contact patch size ranges from $b'/a' = 1/8-1$.

d	b' (mm)		a' (mm)			
25.4 mm (1")	1.00	8.00	6.00	4.00	2.00	1.00
15.875 mm (5/8")	0.63	5.00	3.75	2.50	1.25	0.63
12.7 mm (1/2")	0.50	4.00	3.00	2.00	1.00	0.50
4.763 mm (3/16")	0.09	0.75	0.56	0.38	0.19	0.09

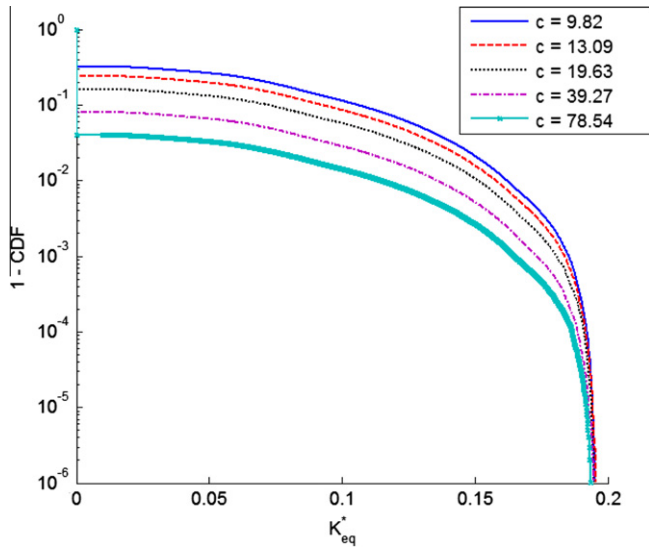


Fig. 10. Cumulative distribution of K_{eq}^* for different conformity values.

4. Conclusions

The present paper presents a comprehensive procedure for evaluating the probability of survival of silicon nitride hybrid ball bearings, under various uncertainties, using surrogate modeling and parametric studies. The surrogate models capture the effects of RCF on SIFs induced at ball surface crack tips and are generated via 3D FEA. The results are of immediate interest and relevance to hybrid ball bearing and turbine engine manufacturers. From this study, the following conclusions can be made:

1. Surrogate modeling using high fidelity SIF from FEA was conducted for swift K_{eq} calculations as a function of crack position, orientation, crack size and maximum contact pressure.
2. The physical observation is used to reduce a multi-dimensional surrogate model to multiple one-dimensional surrogate models, which require less number of samples.
3. It is shown that the cross-validation technique is a good strategy to select the best surrogate model.
4. The parametric study shows that reducing the maximum crack size (by limiting inspection threshold) and increasing the fatigue threshold (by improving fracture toughness of a material) are the most effective ways for reducing the probability of failure. We demonstrate that by decreasing the maximum crack size by 4.4% and by increasing the lowest fracture threshold by 2.8%, the probability of failure is disproportionately reduced by 40%.
5. If the mean crack size (a_{mean}) is proportional to R^x with $x > 1$, then larger balls are less likely to fail; whereas if $x < 1$, smaller balls are superior. We have shown previously that a_{mean} is proportional to $R^{2/3}$ and therefore as the ball diameter decreases survivability increases. This has important implications on hybrid bearing design in terms of selection of ball size and ball complement (number of balls) to support a given load at the desired Hertzian pressure p_0 .
6. Non-dimensionalization technique is used to generalize the bearing survivability for different dimensions and materials.

Acknowledgements

This work was partially supported by the Timken Company, Canton, OH, as a consequence of our research project on critical flaw size evaluation in hybrid silicon nitride ball bearings. We

thank Robert Wolfe of the Timken Co., for discussions pertaining to silicon nitride ball manufacture. We also thank William Ogden and Dr. Herb Chin of Pratt & Whitney, East Hartford, CT, for insight into surface flaw distributions and NDE procedures used in hybrid ball bearing manufacturing.

References

- Allen, M.S., Camberos, J.A., 2009. Comparison of uncertainty propagation/response surface techniques for two aeroelastic systems. In: 50th AIAA/ASME/ASCE/AHS/ASC Structures, Structural Dynamics, and Materials Conference, Palm Springs, CA, May 2009.
- Anderson, T.L., 2005. Fracture Mechanics: Fundamentals and Applications, third ed. CRC Press, Boca Raton, FL.
- Bower, A.F., 1988. The influence of crack face friction and trapped fluid on surface initiated rolling contact fatigue cracks. *J. Tribol.-Trans. ASME* 110, 704–711.
- Cano, J.E., Hernández, L.D., Moral, S., 1996. Importance sampling algorithms for the propagation of probabilities in belief networks. *Int. J. Approx. Reason.* 15 (1), 77–92.
- Chen, Z., Cuneo, J.C., Mecholsky, J.J., Hu, S., 1996. Damage processes in Si_3N_4 bearing material under contact loading. *Wear* 198, 197–207.
- Cundill, R.T., 1997. Impact resistance of silicon nitride balls. In: Niihara, K., Kanzaki, S., Kommeya, K., Morinaga, K. (Eds.), Proceedings of the Sixth International Symposium on Ceramic Materials and Components for Engines. Japan Fine Ceramics Association, Tokyo, pp. 556–561.
- Dassault Systèmes, 2007. ABAQUS Theory Manual, Dassault Systèmes, Providence, RI.
- Evans, A.G., 1983. In: Riley, P.L. (Ed.), Progress in Nitrogen Ceramics. Martinus Nijhoff, Publishers, The Netherlands. p. 595.
- Hadfield, M., 1998. Failure of silicon nitride rolling elements with ring crack defects. *Ceram. Int.* 24, 379–386.
- Hadfield, M., Stolarski, T.A., 1995. The effect of test machine on the failure mode in lubricated rolling contact of silicon nitride. *Tribol. Int.* 28, 377–382.
- Hadfield, M., Stolarski, T., Cundill, R.T., Horton, S., 1993. Failure modes of ceramic elements with ring crack defects. *Tribol. Int.* 26, 157–164.
- Hamrock, B., Dowson, D., 1981. Ball Bearing Lubrication. Wiley-Interscience, New York.
- Harris, T.A., 1991. Rolling Bearing Analysis, third ed. Wiley, New York.
- ISO, 1989. Rolling Bearings – Dynamic Load Ratings and Rating Life, Draft International Standard ISO/DIS 281, 1989, ISO, Geneva, Switzerland.
- Kida, K., Urakami, T., Yamazaki, T., Kitamura, K., 2004. Surface crack growth of silicon nitride bearing under rolling contact fatigue. *Fatigue Fract. Eng. Mater. Struct.* 27, 657–668.
- Kim, N.H., Wang, H., Queipo, N.V., 2006a. Efficient shape optimization under uncertainty using polynomial chaos expansions and local sensitivities. *AIAA J.* 44 (5), 1112–1116.
- Kim, N.H., Wang, H., Queipo, N.V., 2006b. Adaptive reduction of design variables using global sensitivity in reliability-based optimization. *Int. J. Reliab. Saf.* 1 (1), 2102–2119.
- Klemm, H., 2002. Corrosion of silicon nitride materials in gas turbine environment. *J. Euro. Ceram. Soc.* 22 (14–15), 2735–2740.
- Lawn, B.R., 1994. Indentation of ceramics with spheres: a century after Hertz. *J. Am. Ceram. Soc.* 81, 1794–1977.
- Levesque, G., Arakere, N.K., 2008. An investigation of partial cone cracks in silicon nitride balls. *Int. J. Solids Struct.* 45, 6301–6315.
- Levesque, G., Arakere, N., accepted for publication. Critical flaw size in silicon nitride ball bearings, STLE Tribology Transactions.
- Lundberg, G., Palmgren, A., 1947. Dynamic capacity of rolling bearings. *Acta Polytech. Mech. Eng. Ser.* 1 (3), 7.
- Melchers, R., 1999. Structural Reliability Analysis and Prediction, second ed. Wiley, New York.
- Miner, J.R., Dell, J., Galbato, A., Ragen, M.A., 1996. F-117-PW-100 hybrid bearing ceramic technology insertion. *J. Eng. Gas Turb. Power* 118, 434–442.
- Myers, R.H., Montgomery, D.C., 2002. Response Surface Methodology, second ed. Wiley, New York, NY.
- Oguma, N., Sugita, T., Nishi, M., Johns, T.M., 1997. Prediction of brittle failure of silicon nitride ceramics in rolling contact using fracture mechanics. *SAE Paper 2000-01-1339*, pp. 1–14.
- Piotrowski, A.E., O'Brien, M.J., 2006. A novel test method to measure the fracture toughness of ceramic balls used in bearings. *Fatigue Fract. Eng. Mater. Struct.* 29 (7), 558–572.
- Qu, X., Haftka, R.T., 2004. Reliability-based design optimization using probability sufficiency factor. *Struct. Multidiscip. Optim.* 27 (5), 314–325.
- Queipo, N.V., Haftka, R.T., Shyy, W., Goel, T., Vaidyanathan, R., Tucker, P.K., 2005. Surrogate-based analysis and optimization. *Prog. Aerosp. Sci.* 41, 1–28.
- Sadeghi, F., Jalalahmadi, B., Slack, T.S., Raje, N., Arakere, N.K., 2009. A review of rolling contact fatigue. *ASME J. Tribol.* 131, 041403:1–041403:15.
- Shao, M., Badler, N., 1996. Spherical Sampling by Archimedes Theorem, Technical Report, MS-CIS-96-02, Department of Computer and Information Science, University of Pennsylvania, PA.
- Tanimoto, K., Kajihara, K., Yanai, K., 2000. Hybrid ceramic ball bearings for turbochargers, *SAE Paper 2000-01-1339*, pp. 1–14.
- Tu, J.C., 1999. A new study on reliability-based design optimization. *ASME J. Mech. Des.* 121 (4), 557–564.

- Viana, F.A.C., 2009. SURROGATES Toolbox User's Guide. Available from: <<http://fchegury.googlepages.com>>.
- Wang, Y., 2000. Failure Modes of Silicon Nitride Rolling Elements with Ring Cracks, Ph.D. Thesis, Bournemouth University, UK.
- Wang, Y., Hadfield, M., 1999. Rolling contact fatigue failure modes of lubricated silicon nitride in relation to ring crack defects. *Wear* 250, 282–292.
- Wang, Y., Hadfield, M., 2000a. The influence of ring crack location on the rolling contact fatigue failure of lubricated silicon nitride: experimental studies. *Wear* 243, 157–166.
- Wang, Y., Hadfield, M., 2000b. The influence of ring crack location on the rolling contact fatigue failure of lubricated silicon nitride: fracture mechanics analysis. *Wear* 243, 167–174.
- Wang, Y., Hadfield, M., 2001. Ring crack propagation in silicon nitride under rolling contact. *Wear* 250, 282–292.
- Wang, L., Snidle, R.W., Gu, L., 2000. Rolling contact silicon nitride bearing technology: a review of recent research. *Wear* 246, 159–173.